Applied Clay Science 241 (2023) 106950

Contents lists available at ScienceDirect

Applied Clay Science

journal homepage: www.elsevier.com/locate/clay

Research Paper

Electrolysing mud: Membraneless electrolysis of water for hydrogen production using montmorillonite-rich marine mud

C.M.B. Biggs, W.J.F. Gannon, J.M. Courtney, D.J. Curtis, C.W. Dunnill *

Energy Safety Research Institute, 211 ESRI, College of Engineering, Swansea University Bay Campus, Fabian Way, Swansea, Wales SA1 8EN, United Kingdom

ARTICLE INFO

Keywords:
Montmorillonite
Conductivity
Electrolysis
Hydrogen
Efficiency
Alkali

ABSTRACT

This paper describes a design for a low-cost membraneless water electrolyser for the production of green hydrogen that used a viscous electrolyte of naturally abundant montmorillonite-rich marine mud in a DEFT (divergent electrode flow through) geometry with stainless steel (304) mesh electrodes. The ratio of smectite to non-swelling clays in the mud was 1:2. The electrolyte was prepared by resuspending the mud in tap-water to remove the salt, and NaOH 1 M added to enhance the ionic conductivity, as measured by both Electrochemical Impedance Spectroscopy (EIS) and by the slope of DC current/voltage curves. Successful separation and collection of the hydrogen and oxygen gas was inferred from the ratio of 2:1 in the volumes of hydrogen and oxygen collected. Both acid and alkali treatments were trialled and it was found that, whereas acid treatment flocculated the mud, adding NaOH increased the dispersion, conductivity and viscosity, and reduced clogging. The conductivity of both the 24% dry mass alkali mud and a control 4% dry mass alkali bentonite suspension increased to that of pure NaOH 1 M when repeatedly electrolysed. Hydrogen and oxygen gas was collected for 10% and 24% dry mass muds. The less viscous 10% dry mass mud showed turbulent liquid-like behaviour which led to gas mixing but the 24% mud showed stable, solid-like flow and reliable gas separation. Three components of the energy efficiency of the electrolysis process are reported and discussed – the voltage efficiency of 42%, a gas collection efficiency of 50% and the auxiliary power efficiency of 60%. The overall energy efficiency due to these three contributing efficiencies, was 13% of the Higher Heating Value of 142 MJ/kg H_2 for a current density of 45 mA/cm^2. This mud electrolyser may still be considered worth developing for an off-grid, low budget site with a low-power source of renewable energy.

1. Introduction

1.1. Green hydrogen: the current options

Green hydrogen is increasingly seen as a key piece in the global decarbonisation puzzle (Schmidt et al., 2017). The commercial electrolysis of water to produce green hydrogen and oxygen often uses the so-called zero-gap design which consists of two planar and porous electrodes with a thin gas-separation membrane in between (Paidar et al., 2016). The membrane must not conduct electrons or be permeable to oxygen or hydrogen gas, but must conduct one of three ions: H^+ in the case of Proton Exchange Membrane (PEM) acidic membranes such as Nafion, OH^- in the case of alkaline membranes such as Zirfon, or O^{2-} in the case of solid oxide ceramic electrolysers (Buttler and Spliethoff, 2018).

Since Schalenbach et al. (2016) published a near-direct comparison of the performance of Zirfon and Nafion, showing that Zirfon had much lower permeability to hydrogen gas for the same electrical conductivity, and was therefore superior in this respect to Nafion, there has been much development of alkaline electrolysers, which have been the focus of the Swansea University hydrogen group (Passas and Dunnill, 2015; Phillips and Dunnill, 2016; Phillips et al., 2017). Other workers have investigated the most effective catalyst coatings for the electrodes, one of the most cost-effective being Raney Nickel (Gannon and Dunnill, 2019).

Although some novel methods to split water have been developed in recent years, such as introducing a two-step thermochemical cycle (Dotan et al., 2019), direct utilisation of solar energy (Khan et al., 2021), and a capillary-action configuration (Hodges et al., 2022), the pumped water electrolyser remains the central constituent of most green hydrogen production lines (Edwards et al., 2021).

The process of splitting water to form hydrogen and oxygen is very energy-intensive, the Lower Heating Value (LHV) for the endothermic

* Corresponding author.
E-mail address: C.Dunnill@swansea.ac.uk (C.W. Dunnill).

https://doi.org/10.1016/j.clay.2023.106950
Received 4 January 2022; Received in revised form 5 April 2023; Accepted 7 April 2023
Available online 18 May 2023

reaction being 120 MJ per kg of hydrogen using a water-splitting voltage of 1.23 V, and the Higher Heating Value (HHV) being 142 MJ/kg for a thermoneutral reaction using 1.48 V, as it includes the latent heat of vapourisation of water. This energy is in principle recoverable when burning the hydrogen, but in practice there are unavoidable losses in both production and combustion, which are at the heart of the dilemma of whether a hydrogen-based energy economy will be affordable. Nevertheless, it is clear that green hydrogen is needed to replace the grey hydrogen currently used as a chemical feedstock for many industries such as the production of fertiliser and steel.

Operating electrolysers above the water-splitting voltage effectively wastes the excess electrical energy as heat. The resulting dimensionless "voltage efficiency" η for a given water-splitting voltage V has a very simple form. For the HHV value this is:

$$\eta_{HHV} = \frac{1.48}{V} \tag{1}$$

with the equivalent equation for the Lower Heating Value (LHV) efficiency as $1.23/V$. These two voltage efficiencies are therefore in the ratio 1.23/1.48. Commercial alkaline electrolysers are now attaining up to 70% LHV (84% HHV) voltage efficiency (Cihlar et al., 2021), by operating at 30 bar pressure and 80 °C temperature, using KOH 6 M.

With current electricity prices, the bulk of the production costs of hydrogen, with Capex spread over the lifetime of the electrolysis plant, are due to the Opex costs of buying the electrical energy, the remaining being the Capex costs and of supplying the heat and pumping systems. However, with the capability to store hydrogen, it becomes possible to harvest excess renewable energy from off-grid wind turbines and solar panels, and therefore make use of energy which would otherwise be wasted (Gutiérrez-Martín et al., 2010).

However, the cost of commercial membranes is high and some acidic membranes such as Nafion need to be replaced periodically (Borup et al., Oct 2007), increasing the running costs of the electrolyser. This has led authors such as Esposito (2017) to suggest "membraneless" solutions which still ensure gas separation. One such geometry is the DEFT (divergent electrode-flow-through) design where the electrodes are made of a mesh through which the electrolyte flows; this was trialled by Gillespie et al. (2015) using a range of electrodes (pure Ni, Ru/Ir/Ti oxides and Pt) and optimal electrode gaps from 0.8 mm to 2.5 mm, needing pump flow speeds of 0.2 m/s and 0.075 m/s respectively, with 30% mass KOH and an elevated temperature of 70 °C. That study achieved a current density of 101 mA/cm for a voltage of 1.80 V, and therefore an HHV voltage efficiency of 82.2%, comparable to the best alkaline electrolysers (Cihlar et al., 2021).

1.2. Project concept

The impetus for this project was the anticipated large demand for hydrogen and the urgent need to be able to scale up production cheaply. The current direction of research has been to improve both membrane conductivity and electrode materials so as to maximise energy efficiency, but this has led to higher costs for these novel membranes and electrode coatings. The idea for this project was to reduce the cost of the components, but in such a way that the reduction in efficiency could be minimised and the monetary cost of hydrogen kept down. It was decided to look in the natural world for substances that were free at point of extraction, but that still had enough of the desirable properties that made their use worthwhile, especially if scaling up would be easy.

The idea of using clay arose from the knowledge that clay, and especially montmorillonite (Mt), is the only mineral that disperses evenly in water to form a viscous gel and also gives the gel an ionic conductivity elevated above that of the surrounding water: Tabbagh and Cosenza (2007) showed that increasing the proportion of montmorillonite in pure water increases the conductivity of the suspension up to a maximum of 0.45 S/m, or 4.5 mS/cm. Shainberg (1975) similarly studied the conductivity of sodium montmorillonite clay suspensions in salt solutions, and found that for up to 8% mass of clay, the conductivity of the clay suspension in a given salt solution matched that of the salt solution when the electrical conductivity of the whole clay suspension was 2.66 mS/cm. This matched value was therefore given the name of "surface conductivity" and supposed to be due to the mobilisation of water by the action of the clay cations in the plane of the clay. Perhaps coincidentally, the value of 2.67 mS/cm was recorded by McNeill (1980) for the geological deposits with the highest montmorillonite content. These conductivities are of course low compared to that listed for composite electrolysis membranes by Sun et al. (2019), such as 50 mS/cm for some Nafion membranes, but it was considered that with the right chemical treatment the conductivity of the clay could be enhanced.

Rather than attempt to create a solid clay membrane, it was decided to disperse the clay as a mobile electrolyte in DEFT geometry, and to trial both acid and alkali treatments to enhance the conductivity. It was also felt that a viscous electrolyte would separate the hydrogen and oxygen bubbles more effectively than a less viscous electrolyte.

Usually in commercial alkaline electrolysis, KOH is used. However, NaOH is cheaper and much more widely obtainable, and Weiler and Chaussidon (1968), found that sodium montmorillonite gels had a high-frequency Electrochemical Impedance Specroscopy (EIS) conductivity of 4 mS/cm, similar to potassium montmorillonite gels, and that lithium and caesium gels had much lower conductivities of 3 mS/cm and 1 mS/cm respectively. Of the planar clays, both kaolinite and illite are non-swelling clays. In fact, Tabbagh and Cosenza (2007) found that the conductivity of a kaolinite suspension was both very much smaller (4–5 times lower) than that of a montmorillonite suspension and had a smaller increase in conductivity on raising the dry mass percent. Hasan et al. (2018) found that kaolinite and montmorillonite mixtures could be modelled as resistors in a mixture of series and parallel configurations.

Montmorillonite suspensions also have a much higher viscosity than kaolinite suspensions. Kasperski et al. (2011) showed that for a 2% dry mass of clay, the viscosity of Na-montmorillonite in water was 3.622 mPa·s, and the viscosity of 2% Na-kaolinite was 0.920 mPa·s, one-quarter of that of Na-montmorillonite. The same study showed that when mixing kaolinite and montmorillonite, the viscosity of the combined suspension was very close to the sum of the individual viscosities. Thus it was reasoned that natural marine mud, being a mixture of many minerals similar to kaolinite and montmorillonite, would have a viscosity and conductivity dominated by the most viscous and highly conducting mineral component.

The rheological properties of varying mixtures of kaolinite and bentonite have been reported most recently by Shakeel et al. (2021), who showed that the applied shear stress at which the clay mixture transitioned from solid-like to liquid-like behaviour could be changed either by changing the ratio of bentonite to kaolinite or by changing the proportion of water for a given mixture, and that these two variables had a largely equivalent effect.

The effect of pH on both Na- and Ca- forms of kaolinite, illite and smectite have been studied by many workers. A study by Cruz et al. (2013) showed that the addition of alkali further increased this viscosity, especially for high dry mass percentage slurries. Yildiz et al. (1999) showed that the viscosity was higher for both acid and alkali, and Chorom and Rengasamy (1995) showed that the smectite was better dispersed than illite or kaolinite for the same net particle charge, and the zeta-potential (related to the particle charge and giving the degree of dispersion) increased with pH for sodium clays but decreased sharply beyond pH 7.0 for alkaline-treated calcium clays. Calcium montmorillonite also showed less swelling with water than sodium montmorillonite (Segad et al., 2010) and therefore a lower affinity and dispersion in water.

Thus it was decided that clay-rich electrolytes with a significant montmorillonite content, and saturated with sodium ions rather than calcium, would give both a high conductivity and high viscosity, and crucially that any other substances present would not decrease the

desired conductivity and viscosity, so that it would not be necessary to purify the marine mud beyond removing the salt, as the chlorine produced would degrade the anode.

This present study is to our knowledge the first attempt to use an aqueous clay dispersion as an electrolyte for the membraneless production of hydrogen.

2. Materials and methods

2.1. Origin and characterisation of materials

The bulk of the experiments were carried out using marine mud collected from the slipway of Shirehampton Sailing Club on the Somerset Avon between Avonmouth and Bristol, grid reference 2°41′W, 51°29′N which is on the north bank of the Somerset Avon opposite the village of Pill. Allen (1991) reported that the clay composition of sediment across the Severn Estuary was remarkably homogenous, perhaps due to the 13 metre tidal range. In addition, commercial bentonites provided by Clear Off Minerals, clearoffminerals.com (referred to in this paper as Na-Bent1) and Essential Minerals, essentialminerals.co.uk (referred to as Na-Bent2) were obtained as controls. British Kaolinite was also obtained from an online source (mysticmomentsuk.com) and used as a control for the initial viscosity and ex-situ conductivity experiments; XRD analysis showed that this sample was pure.

A quantitative XRD method from Weir et al. (1975) was carried out to determine the ratio of the different minerals within the clay fraction, where the XRD spectra of air-dried mud was compared to that of mud calcined at 300 °C. The XRD spectra were taken on a Bruker D8 Discover in Bragg–Brentano geometry and a 1 D Lynxeye detector. The radiation wavelength was 1.54Å using CuKα with a nickel filter without a monochromator. The slit size was 0.6 mm, taken in steps of 0.02°2θ, with a count time of 0.5 s for each step. The composition of the Shirehampton muds obtained by two different XRD methods as published by Weir et al. (1975) and Fisher and Underwood (1995), are compared with the Severn Estuary and Somerset Avon muds obtained and measured by Allen (1991) in Table 1.

The proportion present of the other minerals (quartz, feldspar and calcite) was also estimated using the intensities of the X-ray diffraction peaks with the calibration method set out by Fisher and Underwood (1995). Table 1 shows that the ratio of swelling clays to non-swelling clays was approximately 1:2. The mud was very fine-grained, with a maximum particle size of 12 μm and some organic matter present.

The Na-Bent1 control was found to contain substantial amounts of quartz, feldspar and calcite so was used only for the acid trials. The Na-Bent2 was much purer so was used as the control for the remainder of the trials. The Na-Bent2 composition from EDX analysis was approximately $Na_{0.4}Ca_{0.04}Al_{1.5}Mg_{0.3}Si_4O_{12}$, which is a layer charge of $-0.43e$ per unit cell, and had a BET specific surface area of 75 m^2/g, which is within the range reported by Kaufhold et al. (2010).

XRD and FTIR spectra of the bentonites and the Shirehampton mud are shown in Fig. 1.

2.2. Preparation of electrolytes

When collected from the Shirehampton slip, the mud was around 50% dry mass and 50% sea-water. Initially, the mud was boiled for 10 min in an excess of tap-water to kill any bacteria, and for later batches, the mud was simply resuspended in cold rainwater or tapwater as the NaOH 1 M was assumed to kill the bacteria (Starliper et al., 2015). To remove the salt, the diluted slurry was settled in a 25-litre tank for several days, the clear supernatant discarded and the remaining 35% dry mass slurry transported to Swansea. EDX and XRD analysis confirmed that the resulting salt content was negligible.

Initially, acid treatment was trialled, but it was found that 0.5 M sulphuric acid treatment both flocculated the mud and reacted with the calcite and organic matter present to produce carbon dioxide and sulphur dioxide. Further trials were carried out on Na-Bent1 which showed that after only two hours of treatment with the 0.5 M H_2SO_4 at room temperature, the sodium had been completely replaced by protons and that the d001-value decreased (thus explaining the flocculation), and an extra O–H stretch peak appeared in the FTIR spectrum, which is attributable to the presence of an H_3O^+ ion.

When the mud was treated with alkali, however, no gas was evolved. The concentration of 1 M NaOH and room temperature treatment was chosen as concentrations of NaOH 5–6 M and/or higher temperatures are known to cause the montmorillonite to either activate as a cement (Khalifa et al., 2020) or dissolve and recrystallise as zeolites as seen by Jeon and Nam (2019) and Elert et al. (12 2015.).

In contrast to the flocculation observed for acid treatment, alkali treatment caused the montmorillonite component to completely delaminate, as observed by the disappearance of the 001 reflection for montmorillonite in the XRD spectra. No new reflections corresponding to zeolite or geopolymer phases were observed to form either before or after electrolysis.

Fig. 1 shows the FTIR results for the acid and alkali treatments.

Although no gas was evolved (as for the acid treatment) the filtrate was yellow in colour and became black when dried at 130 °C. The chemical composition of this yellow fluid as measured by EDX when air-dried was 50 atom% oxygen, 30% sodium and 19.2% carbon with other elements at less than 1%, presumably due to the excess of sodium and the organic matter.

When NaOH was added to the 8% mass control bentonite (Na-Bent2) suspension it became solid-like, and therefore the alkali bentonite suspension was diluted to 4% dry mass.

Several electrolytes were prepared with dry mass percentages ranging from 1% to 30% and are summarised in Table 2.

The ex-situ conductivity before and after electrolysis of both pH 7 and the NaOH 1 M (pH 14) samples was measured using Electrochemical Impedance Spectroscopy (EIS). This used a stand-alone static vertical cell with solid steel electrodes, operating at a low alternating voltage far lower than the voltage required for electrolysis of water to take place. The conductivity was determined by extrapolating the frequency-dependant impedance to its limit at high frequencies where there was zero complex impedance, as this then excluded the contribution from the capacitance of the electrodes.

As viscosity is directly proportional to flow time, the relative flow time of representative samples was determined by measuring the time t for 100 ml of mud to empty through a funnel of fixed width (4.7 mm inside diameter) and column height (5 cm), and dividing this by the time t_{H_2O} for the same volume of pure water (which has a viscosity of 1.006 mPa·s at 20 °C) to drain.

For selected samples, a rigorous rheology assessment was carried out

Table 1
Ratios of minerals in Shirehampton mud, measured by XRD analysis, using methods published by Fisher and Underwood (1995), Weir et al. (1975) and comparing with the compositions of Severn and Somerset Avon found by Allen (1991).

Sample	Montmorillonite%	Illite%	Kaolinite%	Quartz%	Calcite%	Feldspar%
ShireMud (Weir method)	34–47	44–56	8.6–8.7			
ShireMud (Fisher method)	28	45	12	13	2	1
Severn Estuary (Allen)	29	52	14			
Somerset Avon (Allen)	43	36	21			

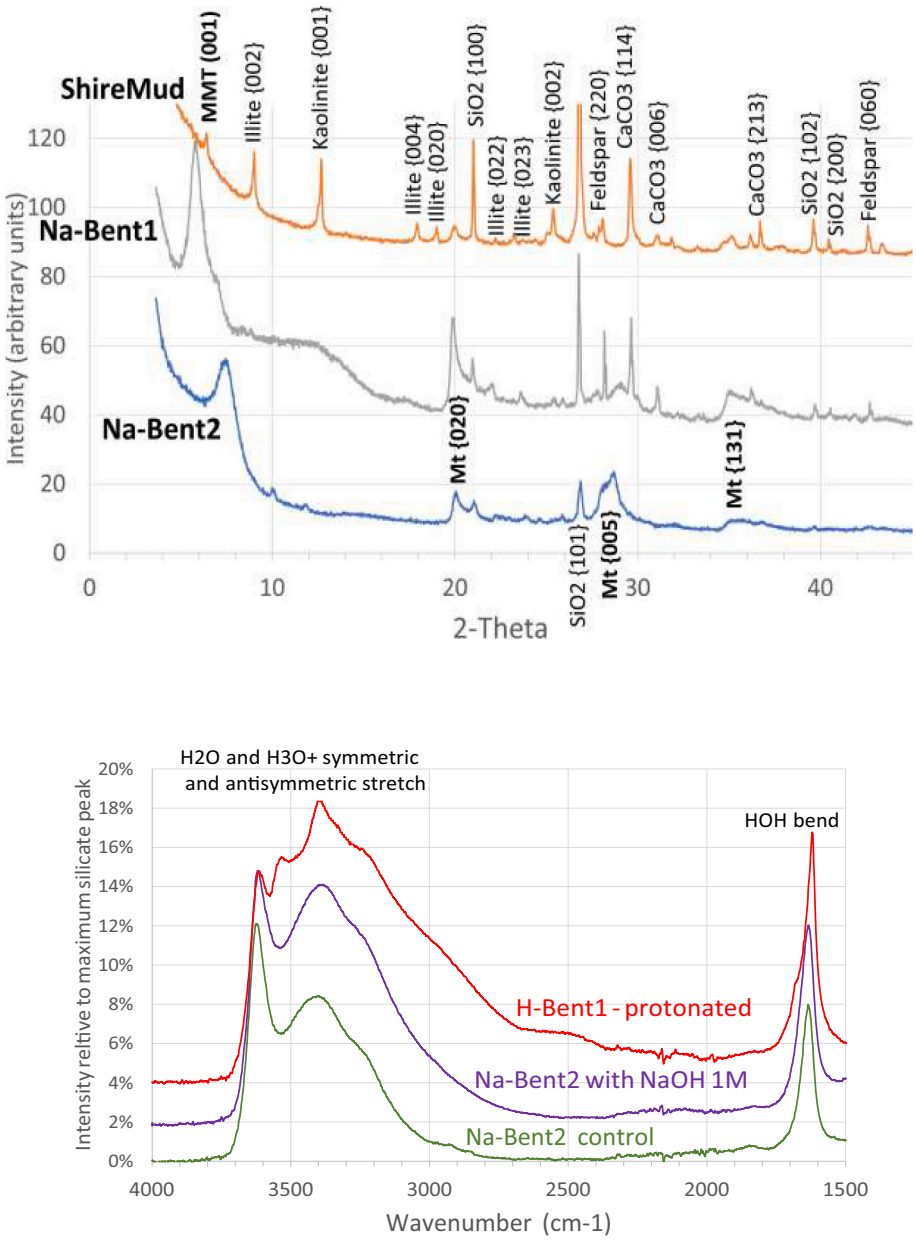

Fig. 1. XRD results for Shirehampton mud and bentonites (top); FTIR results for acid and alkali treatments (bottom).

in a cylindrical rotating geometry, plotting the applied shear stress τ against the rate of strain $d\gamma/dt$. The extracted apparent static yield stress τ_{static} is given in Table 2. Full details of the rheology measurements are given in the Supplementary Material.

Samples with pH 7 (using tap water) were used for initial tests, and pure samples of kaolinite and Na-Bent2 bentonite were used for the viscosity and initial conductivity measurements. Electrolysis tests were carried out on both the alkali-treated Shirehampton muds and the Na-Bent2 4% dry mass bentonite. The concentration of NaOH 1 M was obtained by dissolving 1 mol of NaOH powder in each litre of total slurry volume.

The main sample variable chosen for the electrolytes was dry mass percent. This was controlled by varying the water content, and was determined by measuring the total mass of the mixture after drying in a petri-dish in an oven at 130 °C for 2 h, subtracting the known 4% mass of NaOH, and expressing this as a percentage of the total mass before drying. For a typical 24% mass slurry, the mass of water lost after 2 h of drying was 99.6% of the total water content.

2.3. Cell design

Fig. 2a shows a photograph of the electrolysis cell, with the colourless pipe being one of the two symmetrically-placed mud inlets, and the blue and red pipes being the oxygen- and hydrogen-carrying mud outlets emerging from the anode and cathode respectively. The total closed-loop mud circuit, based on the DEFT design of Gillespie et al. (2015), is shown diagrammatically in Fig. 2b.

In order to keep costs low, the electrodes were made of SAE 304 grade stainless steel mesh (containing 18–20% chromium and 8–10% nickel), with an external surface area of 7 cm × 8 cm = 56 cm^2. A range of mesh sizes were trialed and "14-mesh" selected as it had optimal mud flow. This mesh had a hole size of 1.3 mm and a wire thickness of 0.5 mm, which covered 50% of the total surface area. Results from Phillips et al. (2017) which used the same stainless steel as a solid plate, still with NaOH 1 M but with a Zirfon membrane, and interpolated to a 6 mm electrode spacing, are shown in Fig. 4 for comparison.

A range of electrode gaps from 2 mm to 9 mm were trialled with the

Table 2
Description of electrolyte batches. σ_{EIS} is the conductivity as measured by Electrochemical Impedance Spectroscopy in a test cell with solid steel electrodes, σ_{DC} is the conductivity as measured in the electrolyser cell from the slope of the DC voltage/current curve. Viscosity was measured by the time for a fixed volume of sample to drain through a funnel (t), divided by the time t_{H_2O} for pure water to drain from the same funnel, and by the apparent static yield stress τ_{static} for selected samples. The full rheological description is in the Supplementary Material.

Batch name	pH	Dry Mass %	t/t_{H_2O}	τ_{static}(Pa)	σ_{EIS}(mS/cm)	σ_{DC}(mS/cm)
Na-Bent2 4% in tap-water	pH 7	4%	1.2		2.76	–
Na-Bent2 8% in tap-water	pH 7	8%	2.4		–	3.77
Kaolinite 24% in tap-water	pH 7	24%	0.9		0.804	–
ShireMud 9% in tap-water	pH 7	9%	1.1		4.32	3.99
ShireMud 23% in tap-water	pH 7	23%	1.4		3.22	3.66
Tap-water control	pH 7	0%	1.0		0.26	0.24
NaOH 1 M control	pH 14	0%	1.1		140	53.6
Na-Bent2 4% in NaOH 1 M	pH 14	4%	1.3	4.7	120	30.0
ShireMud 5 litres pre-electrolysis	pH 14	24%	2.0	4.6	108	27
ShireMud 5 litres post-electrolysis	pH 14	24%	2.9		78	30.0
2Vat10%a 50 litres gas collection	pH 14	10%	0.97	0.17	122	27.9
2Vat24%a 50 litres week 1	pH 14	24%	1.7		73	34.3
2Vat24%a week 2 gas collection	pH 14	24%	2.3		99.6	22.6

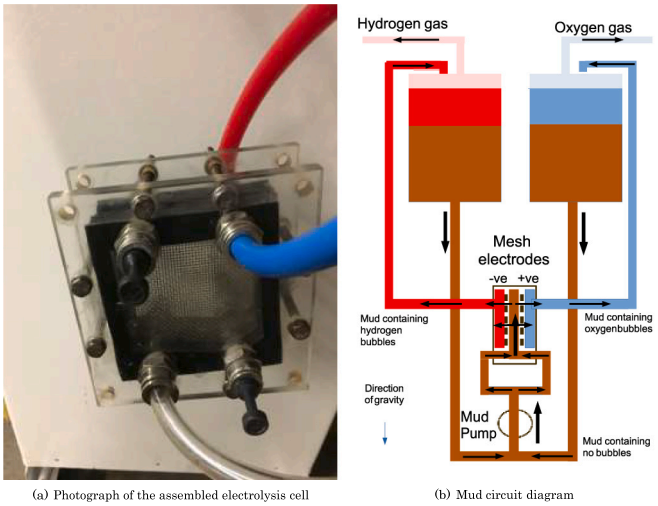

(a) Photograph of the assembled electrolysis cell (b) Mud circuit diagram

Fig. 2. Mud electrolyser design (two vats, closed circuit). Red, on left: mud containing hydrogen bubbles; blue on right, mud containing oxygen bubbles; brown, mud with no bubbles; pink, hydrogen gas; light blue, oxygen gas.

pH-neutral suspensions. Fig. 3 shows the variation of voltage efficiency (determined by interpolating the voltage for a current density of 9 mA/cm^2) with electrode spacing. An electrode spacing of 6 mm was chosen as this gave better mud flow than the more energy-efficient 4 mm spacing.

The diaphragm mud pump used had a variable voltage from 0–9 V and a regulator keeping the current to 1 A. The pump was placed at a point after the mud from two vats was combined into a single stream so that the gravitational pressure assisted the pump in squeezing the mud into the space between the electrodes and out through the mesh. Fig. 3 shows the variation of mud flow rate in litres per second (measured by timing the mud pouring into a litre bucket) with the pump power. This shows that using a pump power higher than 6 W gave a negligible advantage in pump flow and that the 10% and 24% mass muds gave flow rates in keeping with their viscosity, with some variation before and after electrolysis. The pump power was accordingly adjusted for each sample run to achieve a uniform flow rate of about 0.75 litres per minute, with a higher power for more viscous muds. As the inside diameter of the piping used was 10 mm, this flow is equivalent to 0.159 m/s, within the range of 0.075–0.2 m/s speeds used by Gillespie et al. (2015).

For gas collection, each vat was sealed with a gas outlet at the top which took each gas into inverted beakers over water for hydrogen and oxygen volume measurement respectively. A measurement was made of the hydrogen and oxygen volume after about one hour, and the elapsed time, average current, voltage and pump power recorded in Table 3. A water-splitting voltage of 3.5 V was chosen for the gas collection as this gave the optimum "partial power efficiency" (the combination of voltage efficiency and pump power efficiency, but not including gas collection efficiency, as defined later in this paper by Eq. (7) and plotted in Fig. 7).

3. Results

3.1. Results for viscosity and conductivity

Table 2 gives the pH, dry mass percent, viscosity and conductivity of a representative set of electrolytes, where the conductivity was measured by both Electrochemical Impedance Spectroscopy (using AC current with solid steel electrodes) and from the high-current gradient of the I/V curve using the electrolyser cell with DC current (Eq. (2)). The EIS measurement for the NaOH 1 M control (140 mS/cm) was much closer to the 180 mS/cm measured by Rumble (2021) than the DC measurement of 53.6 mS/cm from Table 2, but this is to be expected as the EIS measurement was carried out at very low voltage where bubbles were not being evolved, and bubbles are well known to increase the effective resistance (Phillips and Dunnill (2016)). The DC and EIS measurements for the pH 7 samples can be seen to be much closer to each other and to the literature range of 2–4 mS/cm (Shainberg, 1975).

As a measure of viscosity, the relative flow time t/t_{H_2O} (as measured from the time for a given sample volume to drain through a funnel, divided by the time for pure water to flow) is also shown in Table 2. It can be seen that the 10% dry mass muds had a relative flow time close to 1.0, so were similar to pure water, and the maximum relative flow time of the 24% muds was approximately 3 times that of water. The relative flow time for the 24% alkali-treated mud was similar to that of 4% alkali-treated bentonite. The viscosity of the kaolinite sample was much lower than for the muds and bentonites, as expected from the literature (Shakeel et al., 2021).

The rheological stress/strain measurements showed that the Na-Bent2 4% control slurry in NaOH 1 M had an apparent static yield stress τ_{static} of 4.7 Pa, very close to that of the 24% dry mass alkali Shirehampton mud (4.6 Pa), and that the 10% alkali mud had a very low apparent yield stress. Thus the two hydrogen collection muds of 2Vat10% and 2Vat24% showed very different rheological characteristics, with 2Vat24% showing the same "solid-like" behaviour observed by Shakeel et al. (2021) and 2Vat10% showing rheological behaviour which was much more "liquid-like". A full account is given in the Supplementary Material.

Table 2 also shows that all alkali-treated samples have a conductivity

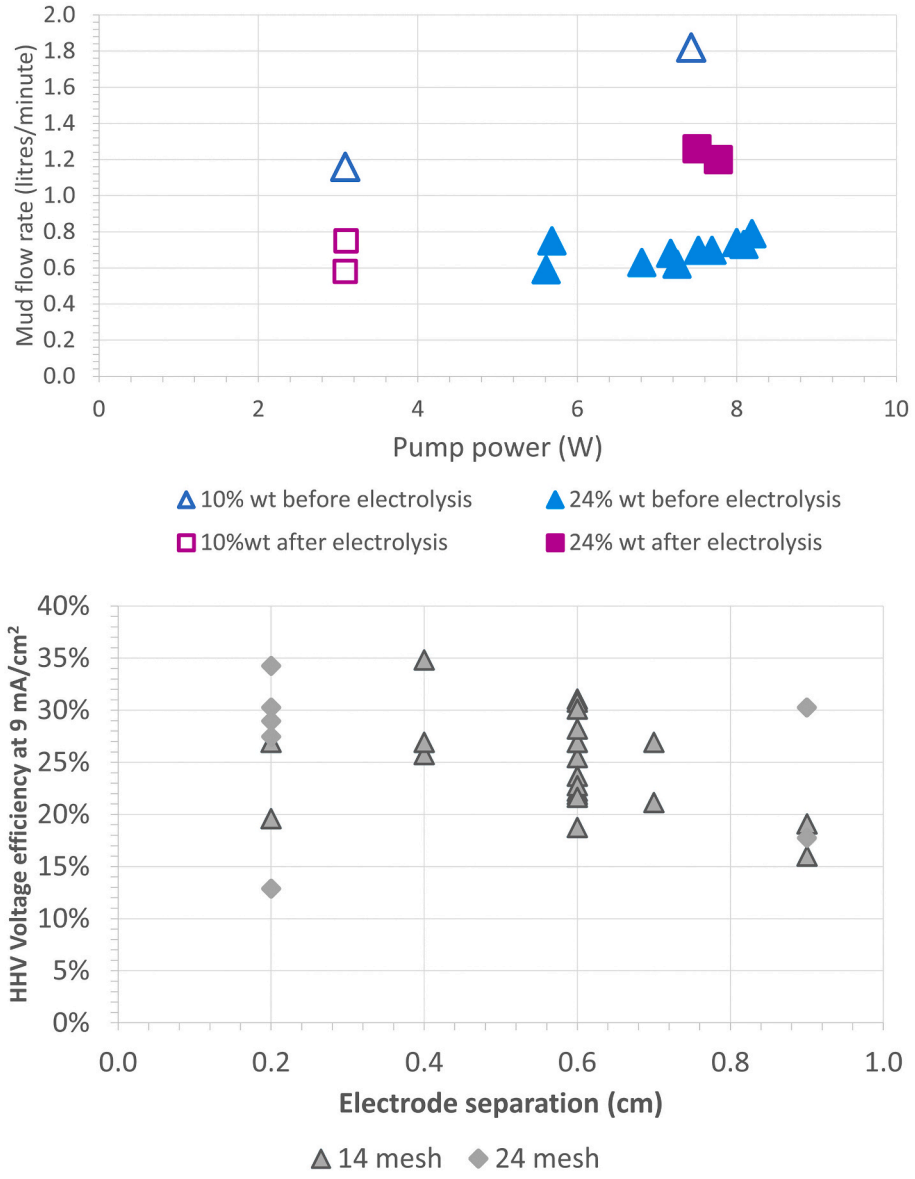

Fig. 3. Mud circuit design trials: Variation of mud flow rate with pump power, and optimising electrode separation and electrode mesh size. 3

much higher than the corresponding pH 7 samples and slightly lower than the conductivity of the pure NaOH 1 M control. As seen later in Fig. 6, when measured in situ during electrolysis, the conductivity rose on repeated electrolysis, and fell when the mud was left to settle.

3.2. *Initial electrolysis observations*

When the electrolysis mesh electrode cell was first trialled with with pH 7 mud in a gravity-driven setup, a major problem was clogging of the electrodes due to lumps in the mud. When the cell was opened up, a reddish-brown discolouration was observed, particularly at the anode, to which the negatively charged clay platelets were seen to be attracted (McKinney and Orazem, 2011). The reddish discolouration was evidence that the iron in the stainless steel electrodes was oxidising at the anode. Fortunately, this would not have affected the hydrogen volume evolved, as the whole cell current also passes through the cathode. On the other hand, no visible chemical changes were seen at the cathode.

The clogging of the pH7 muds was initially reduced using detergent, but it was later found that careful sieving of the few mud clots present rendered this unnecessary. The alkali treatment dispersed the mud and reduced clogging. As a transparent plastic was used for the exterior of the mud cell, it was possible to observe the electrode mesh at the end of a run without opening up the cell, and it could be seen that running water through the cell was sufficient to fully clean the electrodes. However, the alkali control bentonite suspension (4% dry mass) was found to clog the electrodes after a few runs, so it could be that the other minerals present in the Shirehampton muds - such as the kaolinite or the quartz - were helping to carry the mud past the electrodes.

Fig. 4 shows the form of the direct current/direct voltage curve, being a straight line from an intercept on the V-axis, which follows that described by Eq. (2):

$$V = V_0 + IR + b\log_{10}(I) \tag{2}$$

where b is the combined Tafel slope and R the sum of all Ohmic resistances. Differentiating Eq. (2) with respect to I gives:

$$\frac{dV}{dI} = \log_{10}(e)\frac{b}{I} + R = \frac{b'}{I} + R \tag{3}$$

where $b' = 0.4343b$. Inverting this gives

Table 3
Calculation of volume, voltage and energy efficiencies for hydrogen volume collection, using two full vats of mud as in Fig. 2b; 2Vat24%a and 2Vat24%b are repeat measurements taken with 24% dry mass mud; 2Vat10%a and 2Vat10%b are repeat measurements taken with 10% dry mass mud.

	Reference	2Vat24% a	2Vat24% b	2Vat10% a	2Vat10% b
(1)	Voltage	3.5 V	3.5 V	3.5 V	3.5 V
(1a)	Voltage eff% (HHV) = 1.48 V/(1)	42.3%	42.3%	42.3%	42.3%
(1b)	Voltage eff% (LHV) = 1.23 V/(1)	35.1%	35.1%	35.1%	35.1%
(2)	Current	2.42 A	2.70 A	2.65 A	2.49 A
(2a)	Electrolyser power	8.47 W	9.45 W	9.29 W	8.70 W
(2b)	Current density (mA/cm^2) = (2)/56	43.2	48.2	47.4	44.5
(3)	Pump power	5.03 W	6.18 W	2.44 W	6.13 W
(3a)	Pump-only powereff = (3)/((2a)+(3))	63%	60%	83%	59%
(4a)	Partial Power Eff HHV Eq. (7)	26.6%	25.4%	35.1%	24.9%
(4b)	Partial Power Eff LHV Eq. (7)	22.1%	21.5%	21.1%	20.7%
(5)	Time	75 min	20 min	42 min	20 min
(6) h	"Hydrogen" gas volume measured (i.e. from cathode)	600 ml	200 ml	1200 ml	0 ml
(6) o	"Oxygen" gasvolume measured (i.e. from anode)	unknown	100 ml	0 ml	400 ml
(7) h	H_2 vol expected (from 2)	1336 ml	401 ml	802 ml	377 ml
(7) o	O_2 vol expected (7 h/2)	668 ml	200 ml	401 ml	189 ml
(8) h	H_2 volume collection eff% = (6 h)/(7 h)	44.5%	49.9%	150%	0%
(8) o	O_2 volume collection eff% = (6o)/(7o)	unknown	49.9%	0%	300%
(8) c	Total gas collection eff = (6 h + 6o)/(7 h + 7o)	unknown	49.9%	96.7%	106%
(9a)	Total energy efficiency HHV = (4a) × (8 h)	11.8%	12.7%	33.9%	24.1%
(9b)	Total energy efficiency LHV = (4b) × (8 h)	9.83%	10.8%	28.1%	19.9%

$$\frac{dI}{dV} = \frac{I}{b' + IR} \tag{4}$$

This equation shows that for large I, the V/I curve should be straight, as the slope dI/dV becomes equal simply to $1/R$, or the conductance G. As the 14-mesh electrodes had a comparatively low resistance of 23 mΩ (Phillips et al., 2017), the I/V slope therefore was taken to be a fair approximation of the conductance G of the electrolyte alone. The effective DC conductivity of the electrolyte was then calculated from $\sigma = Gd/A$ where A was the electrode area of 56 cm^2 and d was the electrode separation of 6 mm. Another measure of electrolyser effectiveness is the current density in mA/cm^2, being the current I divided by this electrode area, reported in Table 3, row 2b

The V-intercept V_0 of 2.0 V, referred to here as the onset voltage, was the same for all alkali measurements, and it can be seen that the curve indeed became a straight line at higher currents as predicted by Eq. (4), with the gradient giving the total cell conductance $G = 1/R$ of 4.7 S, or resistance of 0.21 Ω. For this cell of surface area 7 × 8 cm^2 and electrode separation 6 mm, this gives a conductivity σ of 50 mS/cm, comparable with that of Nafion and Zirfon membranes as given in Sun et al. (2019). However, as the electrode separation used for commercial cells is much smaller (less than 1 mm), the electrolyte resistance in this study, using an electrode gap of 6 mm, is accordingly much larger. The gradient of the curve measured by Phillips et al. (2017) in Fig. 4 gives 124 mS/cm, which is less than the 180 mS/cm measured by Rumble (2021) for pure NaOH 1 M.

The effective DC conductivity is shown as a function of dry mass percent in Fig. 5, where the data points include the runs where the conductivity increases on repeated electrolysis, as seen later in Fig. 6. For 10% mass alkali muds, the maximum conductivity was lower than for the pure NaOH 1 M, and similar to that for kaolinite, but for low and high dry mass the maximum conductivity was similar to that of pure NaOH 1 M (plotted as 0% dry mass). This increase in conductivity for 24% mass muds and for the 4% mass bentonite control is likely to be due to gel formation in the montmorillonite component, as evidenced by their higher viscosity relative to 10% mass muds in Table 2.

The conductivities of the pH 7 samples shown in Table 2 agree with the results from Shainberg (1975) and Tabbagh and Cosenza (2007) of around 4 mS/cm.

The Swansea laboratory tap-water conductivity was measured in the same apparatus as 0.132 mS/cm for a new electrode and 0.336 mS/com for the same electrode mesh at the end of the six months of operation of

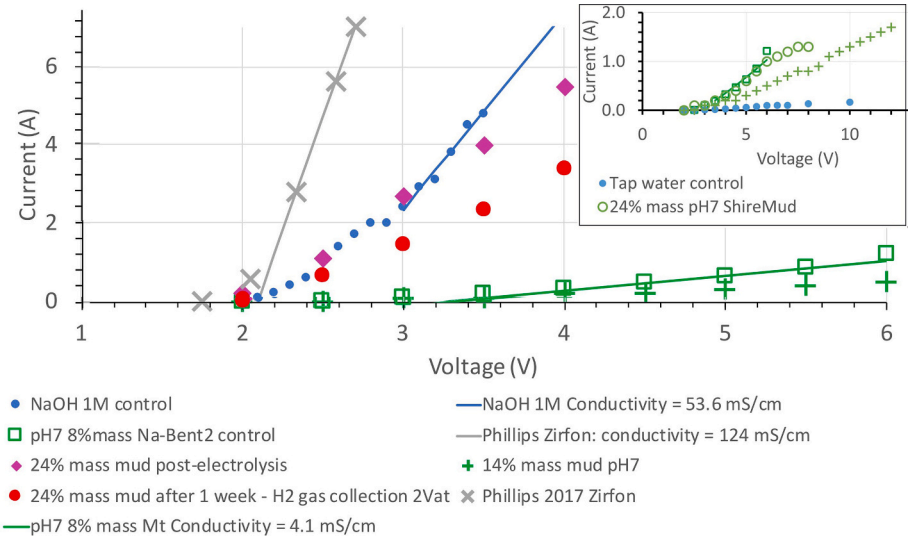

Fig. 4. Comparison of IV curves for NaOH 1 M 24% dry mass alkali mud for selected runs from Table 2, compared with Phillips et al. (2017) electrolysis with NaOH 1 M Zirfon membrane and solid 316-grade stainless steel electrodes for the same electrode gap, and with pH 7 samples. Inset: low-conductivity enlargement of 24% pH 7 mud and tap-water.

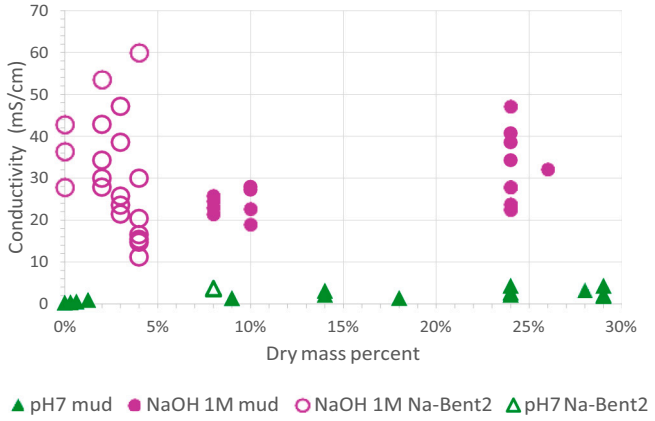

Fig. 5. In-situ DC conductivity of alkali and pH 7 electrolytes as a function of dry mass percent.

the mud cell. This twofold increase in apparent conductivity may be due to an increased catalytic activity in the mesh due to the erosion of the mud increasing its surface area. The same tap-water was measured by EIS with a steel electrode as 0.25 mS/cm, with the Bristol tap-water as 0.75 mS/cm and rainwater as 0.20 mS/cm - all approximately ten times less conducting than the pH-neutral clay-containing electrolytes.

3.3. Consecutive electrolysis measurements

The main electrolysis experiments were carried out with the 14 mesh electrodes, an electrode spacing of 6 mm, and the alkali muds described in Table 2. For each run an I/V curve was obtained using DC voltages in steps of 0.5 V from 0 V to 4.5 V, and the adjusted pump power recorded.

Fig. 6 shows the variation in electrolyser current for continuous electrolysis for a fixed voltage of 3.5 V, including the muds used for the gas collection experiments and two control bentonite suspensions of 3% and 4% dry mass.

For the 5-litre test runs, the conductivity increased up to that of pure NaOH 1 M before reducing. As the electrolyte was seen to become very frothy, the reduction in conductivity could simply be due to the lower density of the frothy electrolyte; this phenomenon is also observed for electrolysers that use membranes and that rely on flow plates to remove the hydrogen and oxygen from the electrode plates (Phillips and Dunnill, 2016).

For the 10% mud (2Vat10% in Fig. 6), the conductivity did not decrease when left to settle or increase when repeatedly electrolysed, but for the 4% bentonite the conductivity was retained after a gap of several weeks, and for the repeatedly electrolysed 4% bentonites, the conductivity increased up to that of NaOH 1 M. The slight overshoot seen above the conductivity of pure NaOH 1 M may be due to the inevitable increase in electrolyte temperature.

When preparing for gas collection using the two 25-litre vats, the first trial (2Vat24%a) was run over two consecutive weeks, and showed that the conductivity of this 24% dry mass electrolyte started high but then reduced when the mud was left to settle at the end of the first week. Fig. 6 showed that the previously higher conductivity of the 2Vat24%a mud was not regained upon repeated electrolysis; this could be a consequence of using a much larger volume of mud and therefore diluting the dispersing effect of the electrolysis on the mud for the same hours of operation.

As the hydrogen collection trials were conducted in the second week, the conductivities of both the 2Vat24%a and 2Vat24%b gas collections were the same as for the 10% mud gas collections (2Vat10%a and 2Vat10%b), enabling easier comparison of the gas collection efficiencies.

3.4. The effect of water-splitting voltage and pump power on energy efficiency

As explained in the Introduction and in Eq. (1), the energy efficiency η from the choice of electrolyser voltage $V_{\text{electrolyser}}$ is equal to the ratio between V and either the Lower Heating Value (1.23 V, if heat is being supplied) or Higher Heating value (1.48 V, if the reaction is to be at constant temperature). Referring to either theoretical voltage as V_{split}, the voltage efficiency η can be written as:

$$\eta = \frac{V_{\text{split}}}{V_{\text{electrolyser}}} \tag{5}$$

If this were the only consideration, then the optimal water-splitting voltage $V_{\text{electrolyser}}$ should be as low as possible. However, this would give a negligible current and therefore a negligible hydrogen flow rate, and as there is also a mud pump running, the pump power would then account for the majority of the system power, giving a poor energy efficiency.

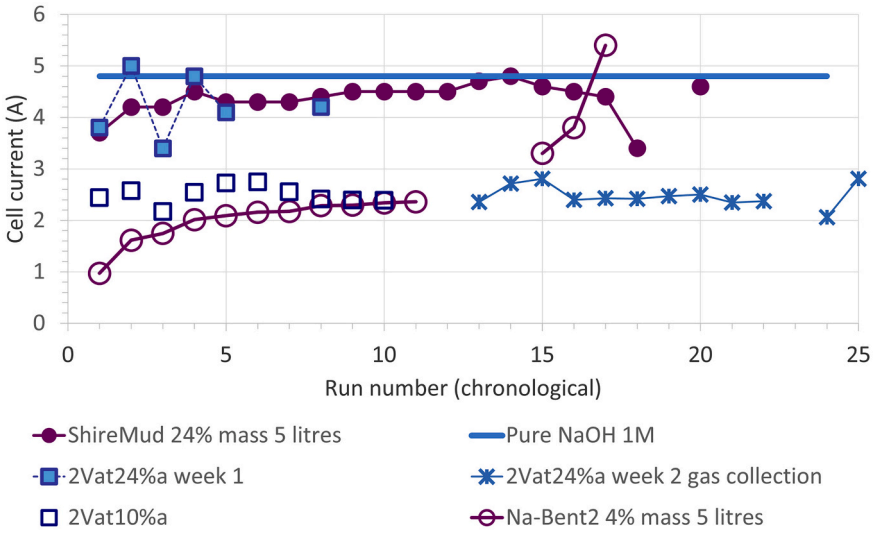

Fig. 6. Cell current for fixed voltage (3.5 V) for repeated electrolysis of alkali mud. A gap of 2 between runs represents a day between runs; a gap of 4 or more represents a week between runs. Batches as described in Table 2. Note that the 2Vat24%a runs are of the same 50-litre batch, in weeks 1 and 2, and the week 2 batch corresponds to the first gas collection.

The "pump-only power efficiency" equation given here:

$$\text{Pump-only power efficiency} = \frac{(VI)_{\text{electrolyser}}}{\left(P_{\text{pump}} + (VI)_{\text{electrolyser}}\right)} \quad (6)$$

assumes that all the power flowing through the electrolyser is useful power, but according to Eq. (5), only the current multiplied by the theoretical water-splitting voltage V_{split} (=1.48 V for HHV) is useful power as the rest is wasted as heat. Thus, replacing $V_{\text{electrolyser}}$ in the expression above by the HHV water-splitting voltage $V_{\text{split}} = 1.48$, and then rewriting this in terms of the voltage efficiency η, gives a "partial power efficiency" for cases like these where the collected hydrogen volume (the third factor to be considered here) has not necessarily been measured. This uses only the voltage and current of the electrolyser, and the electrical power P of the pump, and can be expressed as the product of the two efficiencies, η from Eqs. (5) and (6):

$$\text{Partial power efficiency} = \frac{(VI)_{\text{split}}}{\left(P_{\text{pump}} + (VI)_{\text{electrolyser}}\right)} = \eta x \frac{(VI)_{\text{electrolyser}}}{\left(P_{\text{pump}} + (VI)_{\text{electrolyser}}\right)} = \eta x \text{Pump-only power efficiency} \quad (7)$$

When this Partial Power Efficiency (PPE) was plotted for the highest-conductivity runs for each electrolyte, as a function of water-splitting (i.e. electrolyser cell) voltage, Fig. 7 shows a maximum for this efficiency at a water-splitting voltage of 3.5 V for most of the 24% mass muds and the 4% bentonite suspension, and 3 V for both pure NaOH 1 M and the pH-neutral mud. This maximum efficiency is due to the balance of the two above efficiencies as electrolyser voltage increases - the voltage efficiency (Eq. (1)) reducing and the "pump-only power-efficiency" (Eq. (6)) increasing. The value of the optimal water-splitting voltage of 3.5 V for this system would reduce, and the efficiency improve, if the diaphragm pump were replaced by a more energy-efficient one.

Fig. 7 shows the same Partial Power Efficiency plotted instead as a function of pump power, and shows that as expected, the higher the pump power for constant water-splitting voltage, the lower the partial power efficiency, but the decrease in efficiency was small as the pump power is somewhat lower than the electrolyser power.

3.5. Case study: hydrogen capture results for Shirehampton mud

Table 3 shows the result of the four hydrogen collection experiments,

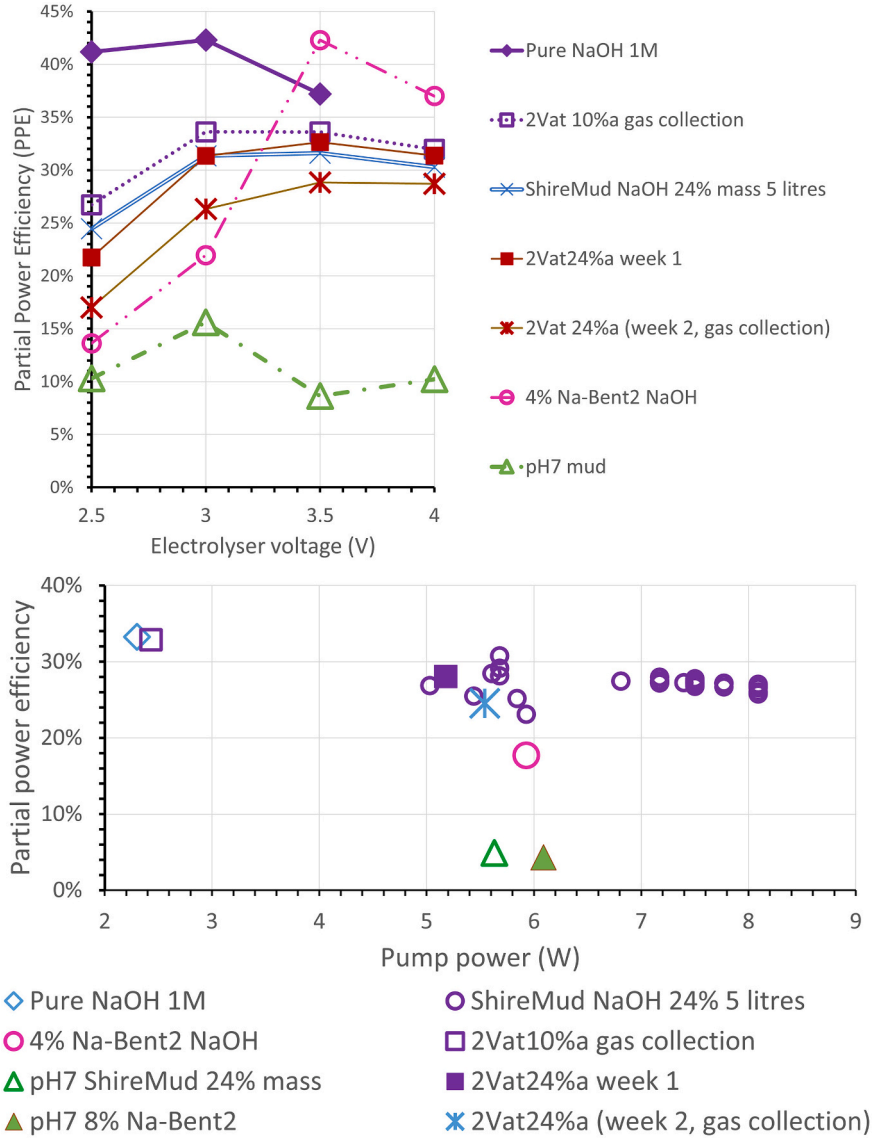

Fig. 7. The variation of Partial Power Efficiency as a function of (top) electrolyser voltage and (bottom) pump power.

which shows two repeat experiments (*a* and *b*) with each of two mud viscosities (24% and 10% dry mass) trialled, labelled with the prefix '2Vat' as this used both large vats as in Fig. 2b. The current density (average 45 mA/cm^2) is also recorded.

The much lower energy efficiency for the 24% mass muds relative to 10% muds is due to the 50% gas collection efficiency (due to retention of bubbles in the mud) and the higher pump power needed for the more viscous muds. However, the ratio of the hydrogen and oxygen (cathode and anode) volumes can be seen to be 2:1, as expected for water electrolysis, which infers that the hydrogen and oxygen gas streams have been successfully separated.

For the two 10% mass runs, the first run showed no gas collection from the anode, and the second showed no gas collection from the cathode, but the total volume of gas collected was equal to the sum of the expected hydrogen and oxygen volumes. Subsequent observation of the two mud streams from cathode and anode outlets from the electrolyser showed mud pouring out of one of the outlets only, which could be reversed by temporarily blocking that outlet. This meant that the hydrogen and oxygen gases were being combined, which is suboptimal for safe storage of hydrogen.

By contrast, for the 24% mass muds, the mud flow was stable and divided equally between the two outlets. The much lower gas collection efficiency of 50% for hydrogen could be seen to be due to gas bubble retention in the mud, and it was also observed that the mud exiting the bottom of the two vats became frothy after a long time, showing that although the gases were not being mixed while exiting the electrolyser (as for the 10% muds), they were instead being remixed when re-entering the pump. This would be resolved by using a larger volume of mud and improving the extraction of bubbles from the mud by mechanical means.

The overall power efficiency was calculated as the Partial Power Efficiency multiplied by the gas collection efficiency, and shown in the final two rows of Table 3. Selecting the second column (2Vat24%b) as the one experiment that successfully separated the hydrogen from the oxygen and also measured both gas volumes, the final energy efficiency was 10.8% if considering the endothermic LHV voltage (1.23 V) and 12.7% if considering the thermoneutral HHV (1.48 V). This includes the lower conductivity due to reflocculation of the mud when allowed to settle over time as seen for the Week 2 for 2Vat24%a in Fig. 6.

4. Discussion

4.1. The effect of electrolysis on the properties of mud

Whether or not this study leads to the design of a viable low-cost water electrolyser for the production of hydrogen, there were some interesting results as regards the conductivity and viscosity of both the mud and the control bentonite suspensions when being pumped through a mesh electrolyser with water splitting voltages ranging from 2.5 to 4.5 V.

Figs. 5 and 6 show that the effective conductivity of the suspension changed not only with the dry mass percent of the mud, but increased on repeated electrolysis, and reduced when the mud was left to settle. It seems therefore that the process of electrolysis further dispersed the clay in the mud. The fact that the 4% dry mass alkali bentonite suspension (Na-Bent2 NaOH 1 M) also increased in conductivity when electrolysed repeatedly, suggests that this behaviour was attributable to delamination and gel formation of the montmorillonite contained in the Shirehampton mud. The dissolution of clay and recrystallisation as other minerals, found at higher temperatures and at higher concentrations of alkali by Elert et al. (12 2015.) and Jeon and Nam (2019), was not evidenced in the X-ray spectra for this study.

When considering the rheological transition between solid and liquid-like phases reported by Shakeel et al. (2021) it seems clear that the 10% Shirehampton alkali mud, which had a low yield stress (see Table 2), behaved in a liquid-like manner, and that both the 24% alkali mud and 4% alkali bentonites, which had similarly high yield stresses, behaved in a solid-like manner when under low yield stress. As repeated electrolysis increased the conductivity of both the 4% bentonite and the 24% alkali mud, but not for the 10% alkali mud, the increase in conductivity must have been due to the further development of a gel network by the montmorillonite platelets.

Finally, the fact that the 24% muds then reverted to the same conductivity as the 10% muds when allowed to settle (week 2 in Table 6), suggests that this gel formation was not permanent but that relamination and flocculation of the clays were taking place.

As the pure bentonite suspensions could not be used for hydrogen collection due to their propensity to clog in the electrolyser, it is likely that the other minerals present in the Shirehampton mud played a role in preventing clogging. Future studies should incorporate such minerals in order to fully reproduce (and improve) this system.

4.2. Comparison of energy efficiency with other electrolyser systems

The 13% overall HHV, 11% LHV energy efficiency obtained here was clearly far lower than the 70% (LHV) or 85% (HHV) efficiency obtained with commercial electrolysers (Cihlar et al., 2021), or the HHV of 83% by Gillespie et al. (2015), as both use sophisticated electrodes and high temperature, pressure and electrolyte concentration. The current density of 45 mA/cm^2 is also relatively low. In a situation where electricity has to be paid for over a period of time and where the financial capital and high-voltage power supply is available, it is clearly preferable to invest in one of the many commercial electrolysers available, as over time the energy efficiency would dominate the overall cost.

This low energy efficiency is due to compounding factors: not only did the high viscosity of the mud (shown to be needed for effective gas separation) retain the gas bubbles from being extracted easily in the vat, but the higher viscosity also meant a higher pump power was needed, giving rise to the observed maximal "partial power efficiency" (PPE) (Eq. (7)) at the water-splitting voltage of 3.5 V. Improving the pump efficiency would lower this optimal water-splitting voltage and therefore increase the voltage efficiency as well.

The main limitation of this method was the high observed onset voltage of 2.0 V, as compared to the thermoneutral voltage of 1.48 V. This was most likely due to poor reaction kinetics at the electrodes as well as the 50% surface area of the mesh, and would be improved by using a more sophisticated electrode material, such as nickel or platinum. However, mud flowing through the mesh could well wear any easily removable coating off.

The option of simply increasing temperature and NaOH concentration as for commercial electrolysers would not be advisable for this mud electrolyser as clay treated with 5–6 M alkali is known to turn into cement (Khalifa et al., 2020). Operating this mesh electrolyser with pure aqueous NaOH 1 M (i.e. with no membrane or clay) would result in bubbles from anode and cathode coalescing together; Gillespie et al. (2015) used saturated KOH which is far more viscous. The turbulent, liquid-like behaviour observed of the less viscous 10% dry mass muds suggests that the fluid rheology of the 24% dry mass muds plays a key role in stabilising the electrolyte flow through the electrodes.

The problem of retention of gas bubbles in the 24% mud could be overcome by a mechanical method or using partial vacuum. Alternatively, a valve system to prevent the diversion of the 10% mud through one outlet only could be investigated.

5. Conclusions

The aim of this research was to find a low-cost method to produce green hydrogen by the electrolysis of water, by removing the necessity to use a commercial gas-separation membrane and instead using a viscous flowing electrolyte which both conducted ions (in this case, OH^-) to enable electrolysis to take place, and to separate the hydrogen and oxygen gases from each other. This was tackled by identifying a source for

the viscous electrolyte which was naturally abundant (in this case being montmorillonite-rich marine mud), and restricting the treatment of this mud to desalination, adding NaOH to a concentration of 1 M, using a stainless steel (SAE 304) 14-mesh electrode and using a diaphragm pump to circulate the mud.

Alkali treatment led to better dispersion of the clays whereas acid treatment flocculated the clays and evolved gas. The alkali treatment also increased the mud conductivity and viscosity relative to the pH-7 muds. The viscosity of the 24% dry mass Shirehampton alkali-treated mud was the same as that of the relatively pure 4% dry mass alkali-treated sodium bentonite, as shown by the very similar yield stresses (4.6 and 4.7 Pa respectively in Table 2) and relative flow times. It was therefore inferred that the montmorillonite in the Shirehampton mud was the dominant active ingredient causing the high viscosity and conductivity needed for this mud electrolyser to work.

Successful separation of hydrogen and oxygen gas using the viscous 24% mud was inferred by the ratio of 2:1 in gas volumes collected from cathode and anode respectively (Table 3). Additionally these more viscous muds increased in conductivity up to that of pure NaOH 1 M when repeatedly electrolysed. As the conductivity decreased when allowing the mud to settle, it was supposed that the rise in conductivity was due to the montmorillonite delaminating and forming a gel network, and then re-flocculating upon settling of the mud over time.

Energy efficiency was evaluated for three components, being the voltage efficiency, the pump-only power efficiency, and the gas collection efficiency. By combining the first two efficiencies into a Partial Power Efficiency and plotting this as a function of water-splitting voltage, the optimal voltage of 3.5 V for this system, or an HHV voltage efficiency of 42%, was deduced (Fig. 7).

However, the pump power needed for the more viscous muds gave an average pump-only power efficiency of 60%. Combining this with the optimised voltage efficiency of 42% and gas collection efficiency of 50% gave a best total energy efficiency of 12.7% (relative to the Higher Heating Value) or a Lower Heating Value energy efficiency of 10.8%, for a current density of 45 mA/cm^2. As the electrolyser uses liquid water throughout, the HHV value would be the correct value to use, but if comparing efficiencies with a fuel cell which uses steam, the LHV value should be used.

Although the 10% dry mass muds needed a lower pump power, the liquid-like flow behaviour due to its low yield stress was turbulent, causing mixing of the hydrogen and oxygen gases, and the conductivity was lower than for 24% muds and did not rise on repeated electrolysis, presumably due to the lack of gel formation.

This mud electrolyser may still be considered worth developing for an off-grid context, where obtaining commercial membranes (or obtaining an electrical solar battery) is not practical and where the CAPEX has to fit a modest budget, provided the low energy efficiency is considered sufficient for the stored energy requirement over a typical day.

CRediT authorship contribution statement

C.M.B. Biggs: Conceptualization, Methodology, Validation, Formal analysis, Investigation, Visualization, Funding acquisition, Data curation, Writing - original draft, Writing - review & editing. **W.J.F. Gannon:** Conceptualization, Methodology, Resources, Writing – review & editing. **J.M. Courtney:** Writing – review & editing. **D.J. Curtis:** Methodology, Validation, Formal analysis. **C.W. Dunnill:** Conceptualization, Methodology, Resources, Writing – review & editing, Supervision, Project administration, Funding acquisition.

Declaration of Competing Interest

The authors declare that they have no known competing financial interests or personal relationships that could have appeared to influence the work reported in this paper.

Data availability

Data will be made available on request.

Acknowledgements

CMBB is grateful for the award of a retraining postdoctoral research fellowship from the Daphne Jackson Trust, and for the joint sponsorship of the Royal Society of Chemistry and the Royal Academy of Engineering.

The authors acknowledge the technical help given by Tom Dunlop with the operation of the X-ray diffractometer and for identifying key components of the clay samples, and by Paul Williams for characterising the particle size distribution of the samples.

Appendix A. Supplementary data

Supplementary data associated with this article can be found, in the online version, at https://doi.org/10.1016/j.clay.2023.106950.

References

Allen, J., 1991. Fine sediment and its sources, severn estuary and inner bristol channel, southwest britain. Sed. Geol. 75 (1), 57–65. URL:https://www.sciencedirect.com/science/article/pii/003707389190050N.

Borup, R., Meyers, J., Pivovar, B., Kim, Y.S., Mukundan, R., Garland, N., Myers, D., Wilson, M., Garzon, F., Wood, D., Zelenay, P., More, K., Stroh, K., Zawodzinski, T., Boncella, J., McGrath, J.E., Inaba, M., Miyatake, K., Hori, M., Ota, K., Ogumi, Z., Miyata, S., Nishikata, A., Siroma, Z., Uchimoto, Y., Yasuda, K., Kimijima, K.-I., Iwashita, N., Oct 2007. Scientific aspects of polymer electrolyte fuel cell durability and degradation. Chem. Rev. 107, 3904–3951.

Buttler, A., Spliethoff, H., 2018. Current status of water electrolysis for energy storage, grid balancing and sector coupling via power-to-gas and power-to-liquids: A review. Renew. Sustain. Energy Rev. 82, 2440–2454. URL:https://www.sciencedirect.com/science/article/pii/S136403211731242X.

Chorom, M., Rengasamy, P., 1995. Dispersion and zeta potential of pure clays as related to net particle charge under varying ph, electrolyte concentration and cation type. Eur. J. Soil Sci. 46 (4), 657–665. URL:https://bsssjournals.onlinelibrary.wiley.com/doi/abs/10.1111/j.1365-2389.1995.tb01362.x.

Cihlar, J., Villar Lejarreta, A., Wang, A., Melgar, F., Jens, J., Rio, P., Leun, K., 2021. Hydrogen generation in Europe: overview of costs and key benefits. Publications Office.

Cruz, N., Peng, Y., Farrokhpay, S., Bradshaw, D., 2013. Interactions of clay minerals in copper–gold flotation: Part 1 – rheological properties of clay mineral suspensions in the presence of flotation reagents. Miner. Eng. 50–51, 30–37.

Dotan, H., Landman, A., Sheehan, S.W., Malviya, K.D., Shter, G.E., Grave, D.A., Arzi, Z., Yehudai, N., Halabi, M., Gal, N., Hadari, N., Cohen, C., Rothschild, A., Grader, G.S., 2019. Decoupled hydrogen and oxygen evolution by a two-step electrochemical-chemical cycle for efficient overall water splitting. Nat. Energy 4 (9), 786–795. https://doi.org/10.1038/s41560-019-0462-7.

Edwards, R.L., Font-Palma, C., Howe, J., 2021. The status of hydrogen technologies in the uk: A multi-disciplinary review. Sustain. Energy Technol. Assess. 43, 100901. URL:https://www.sciencedirect.com/science/article/pii/S221313882031328X.

Elert, K., Pardo, E.S., Rodriguez-Navarro, C., 12 2015.. Mineralogical evolution of di- and trioctahedral smectites in highly alkaline environments. Clays Clay Miner. 63 (6), 414–431. https://doi.org/10.1346/CCMN.2015.0630601.

Esposito, D.V., 2017. Membraneless electrolyzers for low-cost hydrogen production in a renewable energy future. Joule 1 (4), 651–658. URL:https://www.sciencedirect.com/science/article/pii/S2542435117300107.

Fisher, A.T., Underwood, M.B., 1995. Calibration of an x-ray diffraction method to determine relative mineral abundances in bulk powders using matrix singular value decomposition: A test from the barbados accretionary complex. In: Shipley T.H., O. Y., P., B. (Eds.), Proceedings of the Ocean Drilling Program, Initial Reports, vol. 156. pp. 29–37. URL:https://www.researchgate.net/publication/285772896.

Gannon, W.J.F., Dunnill, C.W., 2019. Raney nickel 2.0: Development of a high-performance bifunctional electrocatalyst. Electrochim. Acta 322, 134687. URL: https://www.sciencedirect.com/science/article/pii/S0013468619315580.

Gillespie, M., van der Merwe, F., Kriek, R., 2015. Performance evaluation of a membraneless divergent electrode-flow-through (deft) alkaline electrolyser based on optimisation of electrolytic flow and electrode gap. J. Power Sources 293, 228–235. URL:https://www.sciencedirect.com/science/article/pii/S0378775315009684.

Gutiérrez-Martín, F., Confente, D., Guerra, I., 2010. Management of variable electricity loads in wind – hydrogen systems: The case of a spanish wind farm. Int. J. Hydrogen Energy 35 (14), 7329–7336. URL:https://www.sciencedirect.com/science/article/pii/S0360319910009328.

Hasan, M.F., Abuel-Naga, H., Broadbridge, P., Leong, E.-C., 2018. Series-parallel structure-oriented electrical conductivity model of saturated clays. Appl. Clay Sci. 162, 239–251. URL:https://www.sciencedirect.com/science/article/pii/S0169131718302746.

Hodges, A., Hoang, A.L., Tsekouras, G., Wagner, K., Lee, C.-Y., Swiegers, G.F., Wallace, G.G., 2022. A high-performance capillary-fed electrolysis cell promises more cost-competitive renewable hydrogen. Nat. Commun. 13 (1), 1304. https://doi.org/10.1038/s41467-022-28953-x.

Jeon, I., Nam, K., 2019. Change in the site density and surface acidity of clay minerals by acid or alkali spills and its effect on ph buffering capacity. Sci. Rep. 9 (1), 9878. https://doi.org/10.1038/s41598-019-46175-y.

Kasperski, K., Hepler, C., Hepler, L., 2011. Viscosities of dilute aqueous suspensions of montmorillonite and kaolinite clays. Can. J. Chem. 64, 1919–1924.

Kaufhold, S., Dohrmann, R., Klinkenberg, M., Siegesmund, S., Ufer, K., 2010. N2-bet specific surface area of bentonites. J. Colloid Interface Sci. 349 (1), 275–282. URL: https://www.sciencedirect.com/science/article/pii/S0021979710005278.

Khalifa, A.Z., Cizer, Özlem, Pontikes, Y., Heath, A., Patureau, P., Bernal, S.A., Marsh, A. T., 2020. Advances in alkali-activation of clay minerals. Cem. Concr. Res. 132, 106050. URL:https://www.sciencedirect.com/science/article/pii/S0008884619313420.

Khan, M.A., Al-Shankiti, I., Ziani, A., Idriss, H., 2021. Demonstration of green hydrogen production using solar energy at 28% efficiency and evaluation of its economic viability. Sustain. Energy Fuels 5, 1085–1094.

McKinney, J.P., Orazem, M.E., 2011. A constitutive relationship for electrokinetic dewatering of phosphatic clay slurries. Mining Metall. Explor. 28, 49–54.

McNeill, 1980. Electrical conductivity of soils and rocks. Geonics. URL:http://www.geonics.com/pdfs/technicalnotes/tn5.pdf.

Paidar, M., Fateev, V., Bouzek, K., 2016. Membrane electrolysis—history, current status and perspective. Electrochim. Acta 209, 737–756. URL:https://www.sciencedirect.com/science/article/pii/S0013468616313007.

Passas, G., Dunnill, C., 2015. Water splitting test cell for renewable energy storage as hydrogen gas. J. Fundam. Renew. Energy Appl. 5 (5), 188.

Phillips, R., Dunnill, C., 2016. Zero gap alkaline electrolysis cell design for renewable energy storage as hydrogen gas. RSC Adv. 6, 100643–100651. https://doi.org/10.1039/C6RA22242K.

Phillips, R., Edwards, A., Rome, B., Jones, D.R., Dunnill, C.W., 2017. Minimising the ohmic resistance of an alkaline electrolysis cell through effective cell design. Int. J. Hydrogen Energy 42 (38), 23986–23994. URL:https://www.sciencedirect.com/science/article/pii/S0360319917330203.

Rumble, J.R. (Ed.), 2021. Handbook of Chemistry and Physics Online, 102nd ed. Taylor and Francis. URL:https://hbcp.chemnetbase.com/faces/contents/ContentsSearch.xhtml.

Schalenbach, M., Tjarks, G., Carmo, M., Lueke, W., Mueller, M., Stolten, D., 2016. Acidic or alkaline? towards a new perspective on the efficiency of water electrolysis. J. Electrochem. Soc. 163 (11), F3197–F3208. https://doi.org/10.1149/2.0271611jes.

Schmidt, O., Gambhir, A., Staffell, I., Hawkes, A., Nelson, J., Few, S., 2017. Future cost and performance of water electrolysis: An expert elicitation study. Int. J. Hydrogen Energy 42 (52), 30470–30492. URL:https://www.sciencedirect.com/science/article/pii/S0360319917339435.

Segad, M., Jönsson, B., Åkesson, T., Cabane, B., 2010. Ca/na montmorillonite: Structure, forces and swelling properties. Langmuir 26 (8), 5782–5790. https://doi.org/10.1021/la9036293.

Shainberg, I., 1975. Electrical conductivity of na-montmorillonite suspensions. Clays Clay Miner. 23, 205–210.

Shakeel, A., Kirichek, A., Chassagne, C., 2021. Rheology and yielding transitions in mixed kaolinite/bentonite suspensions. Appl. Clay Sci. 211, 106206. URL:https://www.sciencedirect.com/science/article/pii/S0169131721002301.

Starliper, C.E., Watten, B.J., Iwanowicz, D.D., Green, P.A., Bassett, N.L., Adams, C.R., 2015. Efficacy of ph elevation as a bactericidal strategy for treating ballast water of freight carriers. J. Adv. Res. 6 (3), 501–509 editors and International Board Member collection. URL:https://www.sciencedirect.com/science/article/pii/S2090123215000284.

Sun, X., Simonsen, S.C., Norby, T., Chatzitakis, A., 2019. Composite membranes for high temperature pem fuel cells and electrolysers: A critical review. Membranes 9 (7). URL:https://www.mdpi.com/2077-0375/9/7/83.

Tabbagh, A., Cosenza, P., 2007. Effect of microstructure on the electrical conductivity of clay-rich systems. Phys. Chem. Earth, Parts A/B/C 32 (1), 154–160 clay in natural and engineered barriers for radioactive waste confinement - Part 1. URL:https://www.sciencedirect.com/science/article/pii/S1474706506001914.

Weiler, R.A., Chaussidon, J., 1968. Surface conductivity and dielectrical properties of montmorillonite gels. Clays Clay Miner. 16 (2), 147–155. https://doi.org/10.1346/CCMN.1968.0160205.

Weir, A.H., Ormerod, E.C., El Mansey, I.M.I., 1975. Clay mineralogy of sediments of the western nile delta. Clay Miner. 10 (5), 369–386.

Yildiz, N., Sarikaya, Y., Çalimli, A., 1999. The effect of the electrolyte concentration and ph on the rheological properties of the original and the na2co3-activated kütahya bentonite. Appl. Clay Sci. 14 (5), 319–327. URL:https://www.sciencedirect.com/science/article/pii/S016913179900006X.